THE INTERNATIONAL CONFERENCE ON THE 120TH ANNIVERSARY OF THE BULNAY EARTHQUAKE: ADVANCES IN ASTRONOMY AND GEOPHYSICS

Statistical study of predictive parameters for Geomagnetic Storms during 23-24 solar cycles

B. Tsegmed, B. Namuun

Institute of Astronomy and Geophysics, Academy of Sciences (IAG MAS), Ulaanbaatar, Mongolia

ABSTRACT

This work focuses on exploring the correlation between solar activity parameters and geomagnetic activity during solar cycles **23** and **24**. The analysis includes variables such as solar wind speed (***Vsw***), proton density (***Np***), solar wind dynamic pressure (***Psw***), and components of the interplanetary magnetic field (*Bz* and *By*), along with energy-related parameters (*Esw*, *dφ/dt*, *ε*). Correlation coefficients and time lags were calculated between these solar wind, magnetic field, and energy parameters and geomagnetic indices (*SYM-H*, *AE*) for storms driven by CMEs and CIRs. The analysis of time delays (Δ*t*) of auroral activity relative to the energy parameters and the *Bz* component of the interplanetary magnetic field for both types of storms revealed durations ranging from 30 to 60 minutes, while for the ring current, the delays ranged from 6 to 24 hours.

INTRODUCTION

Geomagnetic storms and substorms are hazardous space weather phenomena that can disrupt power grids, satellite operations, and communication systems. These disturbances are primarily triggered by solar activity—specifically coronal mass ejections (CMEs) and corotating interaction regions (CIRs)—which drive high-speed solar wind streams toward Earth. The collision of the solar wind with our planet's magnetic field leads to the occurrence of geomagnetic storms and substorms.

- The transfer of solar wind energy, momentum, and mass into Earth's magnetosphere occurs primarily through magnetic reconnection at the dayside magnetopause (Paschmann et al., 1979 [1]). However, additional entry mechanisms can include:
- Direct cusp entry (Kremser & Lundin, 1990 [2]),
- Impulsive plasma penetration across the magnetopause (Gunell et al., 2012 [3]),
- Diffusion at the magnetospheric boundary(Tsurutani & Thorne, 1982 [4]),
- High-latitude reconnection and during northward IMF orientation, through the Kelvin-Helmholtz instability (Hasegawa et al., 2004 [5]; Fuselier et al., 2000 [6]).
- For decades, researchers have studied the relationship between solar wind parameters, the interplanetary magnetic field (IMF), and geomagnetic field indices to better understand and predict geoeffective geomagnetic storms. Accurate forecasting is essential to mitigate the risks these storms pose to technological systems. Numerous studies have explored the causes, characteristics, and solar–interplanetary drivers of geomagnetic storms, leading to the development of various prediction models and methods aimed at improving space weather forecasting.
- In our previous study (Namuun, 2023 [26]), we analyzed 131 CME-driven and 161 CIR-driven storms during Solar Cycles 23–24, evaluating the correlation between solar wind/IMF parameters and geomagnetic indices. This work aimed to identify effective predictors and estimate lead times for issuing early space weather warnings.

METHODOLOGY AND DATA

This study utilizes high-resolution (1-minute) interplanetary and geomagnetic data from the OMNI database (https://omniweb.gsfc.nasa.gov), a widely recognized source in space weather research. The OMNI data merges measurements from the ACE, WIND, and IMP-8 spacecraft.
We analyzed solar wind–magnetosphere interactions during Solar Cycles 23 (1996–2006) and 24 (2009–2017). **Key solar wind parameters included:**

- Solar wind speed (**Vsw**)
- Proton density (**Np**)
- Dynamic pressure (**Psw**)
- Total interplanetary magnetic field (**B**)
- IMF components (**By, Bz**)

To evaluate geomagnetic responses, we used several indices:

- **SYM-H** index: A high-resolution (1-minute) variant of Dst (hourly averaged deviation of the horizontal component of Earth's magnetic field), widely used for real-time storm monitoring.
- **AE index**: Measures the intensity of the auroral electrojet, indicating substorm activity. It is derived from 12 high-latitude observatories between 60°–70° geomagnetic latitude (Davis et al., 1966 [22]; Baumjohann & Treumann, 2012 [24]).

These indices collectively allow for comprehensive monitoring of geomagnetic storm and substorm activity in response to varying solar wind and IMF conditions.

ENERGY COUPLING BETWEEN SOLAR WIND AND MAGNETOSPHERE

The combined solar wind parameters represent the energy coupling relationship between the solar wind and Earth's magnetosphere.
The interaction between the solar wind and Earth's magnetosphere is quantified using energy coupling functions, which combine key solar wind parameters to estimate the energy input into the magnetospheric system.
One widely used formulation is the Akasofu ε (epsilon) function—an empirical representation of the solar wind's energy transfer rate, which correlates well with both geomagnetic storms and individual substorms (Akasofu, 1981 [9]). Originally introduced by Perreault and Akasofu (1978 [12]), it is expressed as:

$$\varepsilon = V_{SW} B^2 l_0^2 sin^4(\theta/2)$$

Where:

- V_{SW} : solar wind speed
- B: interplanetary magnetic field strength
- θ: IMF clock angle (angle between IMF and geomagnetic field)
- l_0 : scaling parameter (~7 Earth radii)

This function represents the Poynting flux into the magnetosphere, providing a valuable estimate of geoeffective energy input during disturbed solar wind conditions.

$$\theta = tan^{-1}(|B_y|/|B_z|)\ ,\ B_z > 0,$$
$$\theta = 180^0 - tan^{-1}(|B_y|/|B_z|)\ ,\ B_z < 0$$

The Akasofu function depends not only on IMF clock angle on YZ plane, but also on $V_{sw}B^2$,representing the solar wind electric field that plays an essential role in the magnetospheric convection (Burton et al., 1975, [23]).
Moreover, E_{KL} and $d\varphi/dt$ also depends the solar wind electric field and IMF clock angle.
Moreover, coupling functions such as the Kan–Lee electric field and the Newell coupling function also depend on the solar wind electric field and the IMF clock angle.
The mean electric field at the magnetopause E_{KL}, proposed by Kan and Lee (1979), is expressed as:

$$E_{KL} = V_{sw} B\ sin^2(\theta/2)$$

The Newell coupling function defines the magnetic flux transfer rate across the magnetopause and is given by [Newell et al., 2007]:

$$\frac{d\varphi}{dt} = V_{sw}^{4/3} B^{2/3} sin^{8/3}(\theta/2)$$

To identify causal relationships and determine **time lags** betSween **solar wind (SW) parameters**, **interplanetary magnetic field (IMF)** data, and **geomagnetic indices**, we applied a **cross-correlation analysis** method.
For two continuously varying signals $x(t)$ and $y(t)$ of infinite duration, the **cross-correlation function** c_{xy} at time lag τ is defined by the following integral:

$$c_{xy}(\tau) = \int_{-\infty}^{\infty} x(t)\ y(t \pm \tau) dt$$

If *y(t) = x(t)*, the function is called autocorrelation.
This function measures the similarity between $x(t)$ and the time-shifted version of $y(t)$, allowing us to detect the **delay at which the response (e.g., geomagnetic activity)** is most strongly correlated with a **driving input (e.g., SW parameter)**.
For the classical case of **stationary and ergodic time series** $x(t)$ and $y(t)$, where i =1…n , the **discrete cross-correlation function** c_{xy} is given by:

$$c_{xy}(\tau) = \frac{1}{n-\tau} \frac{\sum_{i=1}^{n-\tau}(x(i) - M_x)(y(i+\tau) - M_y)}{S_x\ S_y}$$

where: M_x, M_y :mean values, S_x, S_y: standard deviations, τ : time lag n: total number of samples
To assess the correlation between solar wind parameters, IMF components, and geomagnetic indices, we applied Superposed Epoch Analysis (SEA). Events were aligned relative to the minimum SYM-H value, marking the main phase of each geomagnetic storm. This method enables the calculation of average parameter behavior before and after storm onset, improving the identification of predictive patterns and lead times.

CROSS CORRELATION ANALYSIS FOR CMEs INDUCED STORM

Variation of the cross correlation calculated between SYM-H index and solar wind, IMF parameters during CME-driven storms at different time lag is shown in figure 1

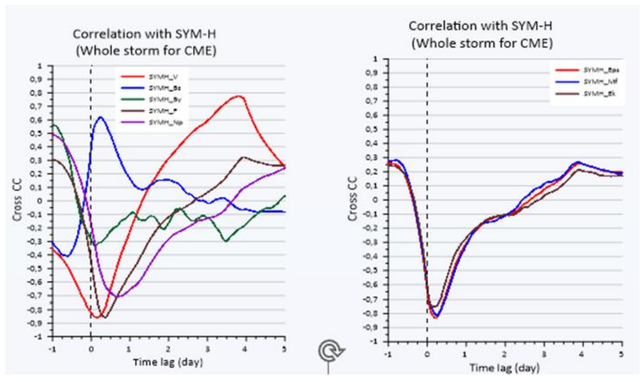

Figure 1

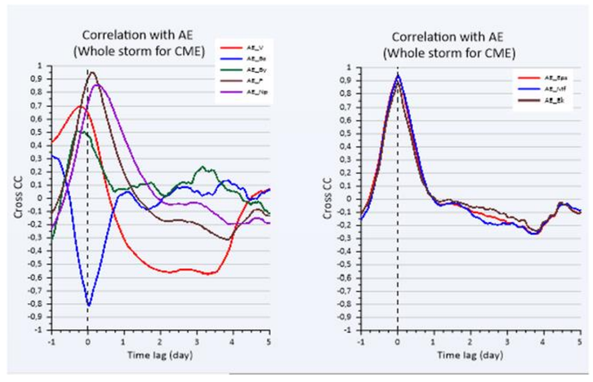

Figure 2

Solar wind velocity shows the strongest correlation with SYM-H (CC = -0.86) at Δt ≈ 216 min (3h36m), indicating SYM-H responds ~3.5 hours after a velocity increase.

- Dynamic pressure (Psw) peaks at Δt ≈ 510 min (8h30m) with CC = -0.86, ~5 hours after velocity and ~8 hours after density.
- Density reaches maximum correlation (CC = -0.71) at Δt ≈ 950 min (15h50m), showing the earliest influence.
- MF Bz shows a moderate correlation (CC = 0.62) at Δt ≈ 350 min (5h50m), suggesting Bz alone may not control SYM-H changes.
- Among coupling functions:
- ε (epsilon) has the highest CC = -0.83 at Δt ≈ 318 min (5h18m). ***Figure 1***

- dϕ/dt (reconnection rate) follows with CC = -0.81 at Δt ≈ 350 min (5h50m).
- EKL function peaks at Δt ≈ 290 min (4h50m) with CC = -0.75.

The IMF - **Bz component** is the earliest trigger for **ring current development**, as indicated by its strong correlation with the **SYM-H index** at a time lag of **Δt = 4h30m (CC = 0.71)**. This aligns with the general understanding that a southward Bz leads to enhanced geomagnetic activity through dayside magnetic reconnection. The IMF-**By component**, although less impactful, shows a moderate correlation (**CC = 0.55**) at **Δt ≈ 12h**. Similarly, the **solar wind speed (Vsw)** presents a strong negative correlation (**CC = -0.86**) with **SYM-H** at **Δt ≈ 8h**, implying its role in the gradual enhancement of the ring current.

- **Dynamic pressure** reaches a strong correlation (**CC = -0.85**) at **Δt ≈ 15h30m**.

Proton density peaks (**CC = -0.67**) at a longer lag of **Δt ≈ 24h45m**, indicating a slower response. **EKL (reconnection electric field)** at **Δt ≈ 4h48m, CC = -0.75**,

- followed by **magnetic flux dϕ/dt** at **Δt ≈ 5h34m, CC = -0.92**,
- and **ponderomotive force ε** at **Δt ≈ 6h, CC = -0.83**.

These suggest that **SYM-H** is strongly driven by both IMF orientation and solar wind energy transfer mechanisms. ***Figure 2***

CROSS CORRELATION ANALYSIS FOR CIRs INDUCED STORM

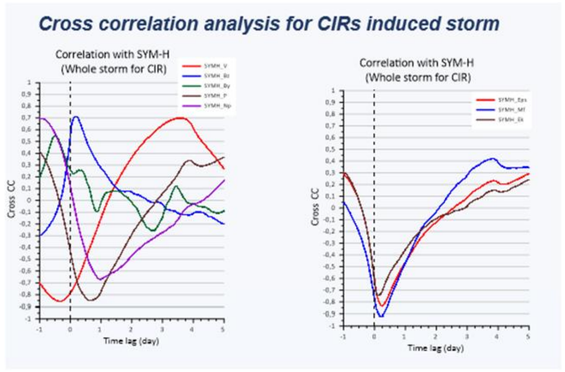

Figure 3

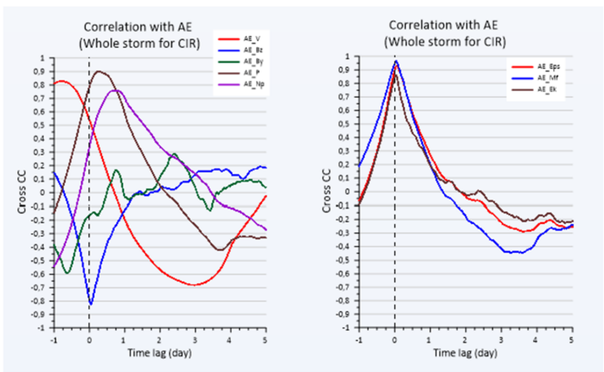

Figure 4

For the **AE-index** (Fig. 4, right), strong correlations were found:

- **Bz**: **Δt = 1h, CC = -0.82**
- **Density (Np)**: **Δt = 18h28m, CC = 0.76**
- **Pressure (Pn)**: **Δt = 6h20m, CC = 0.90**
- **Vsw** shows the strongest AE correlation (**CC = 0.83**) at a large delay (**Δt = 18h35m**).

This delay reflects the velocity structure typical of **Corotating Interaction Regions (CIRs)**, where the wind speed gradually intensifies while other parameters (e.g., density, pressure) decline, especially during the **recovery phase** (Richardson, 1996; 1998).
The **IMF By component** undergoes a directional shift—from **positive to negative**—during the **main and early recovery phases** of geomagnetic storms. This transition is confirmed by a **peak negative correlation (CC = -0.59)** at a **time lag of Δt ≈ -15h**, indicating By influences the magnetosphere **before** SYM-H changes. ***Figure 3***

Ring Current Development During CIR Events
During **Corotating Interaction Regions (CIRs)**, key **solar wind–magnetosphere coupling functions** correlate **negatively** with the SYM-H index, indicating that **as ring current strengthens, the global magnetic field weakens**.
Key coupling responses include:

- **Magnetic flux rate (dϕ/dt):** Strongest correlation (**CC = -0.92**) at **Δt ≈ 5h35m**.
- **Magnetopause electric field (EKL):** Peaks at **Δt ≈ 3h**, with **CC = -0.74**.
- **Ponderomotive force (ε):** Responds at **Δt ≈ 6h**, with **CC = -0.83**.

These correlations demonstrate that **energy dissipation in the solar wind directly feeds into ring current enhancement**, which subsequently drives **geomagnetic storm intensity**, consistent with superposed epoch analyses of storm events. ***Figure 4***

CONCLUSION

A statistical analysis was conducted on 131 CME-driven and 161 CIR-driven storms that occurred during Solar Cycles 23 and 24. The main findings of the analysis are as follows:

1. **For both types of storms, the development of the ring current is strongly influenced by solar wind parameters.** The correlation coefficients are high, approximately -0.85 with solar wind speed (*Vsw*) and dynamic pressure (*Psw*). The correlation with proton density (*Np*) is slightly lower, with coefficients around -0.70. Interplanetary magnetic field (IMF) parameters show weaker correlations compared to solar wind parameters. However, energetic parameters demonstrate quite strong correlations, especially the rate of change of magnetic flux (dϕ/dt), which reaches values greater than -0.92 during CIR-driven storms.
2. **Auroral activity shows a strong dependence on solar wind and IMF parameters,** except for solar wind speed (*Vsw*) in CME-driven storms, where the correlation is weaker (correlation coefficient = -0.69). The *By* component of the IMF shows a stronger correlation with auroral activity than the *SYM-H* index. Energetic parameters correlate strongly in the context of both auroral activity and ring current development.
3. **Time delays (Δt) in auroral activation relative to energetic parameters and IMF *Bz* are very short for CME-driven storms—** about half an hour or less. For CIR-driven storms, the delay is around one hour. In the case of the ring current: for CME-driven storms, the key parameters are *Vsw* and *Bz*; for CIR-driven storms, *Bz* is dominant. In both cases, energetic parameters show development times ranging from 3 to 6 hours on average, while solar wind parameters such as *Psw* and *Np* show delays ranging from 12 hours to a full day. For auroral activity, the average delay is also 3 to 6 hours, except for *Vsw* and *Np* during CIR-driven storms.

REFERENCES

1. **Paschmann, G., Sonnerup, B., Papamastorakis, I. et al. Plasma acceleration at the Earth's magnetopause: evidence for reconnection. Nature 282, 243–246 (1979). https://doi.org/10.1038/282243a0.**
2. **Kremser, G., and R. Lundin (1990), Average spatial distributions of energetic particles in the midaltitude cusp/cleft region observed by Viking, *J. Geophys. Res.*, 95(A5), 5753–5766, doi:10.1029/JA095iA05p05753.**
3. **Gunell, H., Nilsson, H., Stenberg, G., Hamrin, M., Karlsson, T., Maggiolo, R., André, M., Lundin, R., and Dandouras, I.: Plasma penetration of the dayside magnetopause, Phys. Plasmas, 19, 072906, doi:10.1063/1.4739446, 2012.**
4. **Tsurutani, B.T. and Thorne, R.M. (1982). Diffusion processes in the magnetopause boundary layer. *Geophysical Research Letters 9: doi: 10.1029/GL009i011p01247. issn: 0094-8276.***
5. **Hasegawa, H., Fujimoto, M., Phan, TD. *et al.* Transport of solar wind into Earth's magnetosphere through rolled-up Kelvin–Helmholtz vortices. *Nature* 430, 755–758 (2004). https://doi.org/10.1038/nature02799**
6. **Fuselier, S. A., R. Frahm, W. S. Lewis, A. Masters, J. Mukherjee, S. M. Petrinec, and I. J. Sillanpaa (2014), The location of magnetic reconnection at Saturn's magnetopause: A comparison with Earth, *J. Geophys. Res. Space Physics*, 119, 2563–2578, doi:10.1002/2013JA019684.**
7. **B. Namuun, B. Tsegmed, L. Y. Li, and G. M. Leghari, "Differences in the response to CME and CIR drivers of geomagnetic disturbances", Solnechno-Zemnaya Fiz., vol. 9, no. 2, pp. 35–40, 2023, doi: 10.12737/szf-92202304.**